European Journal of Physics

Geodetic model for teaching motion on the Earth's spheroidal surface

To cite this article before publication: Boyd F. Edwards *et al* 2021 *Eur. J. Phys.* in press https://doi.org/10.1088/1361-6404/ac0e87

Geodetic Model for Teaching Motion on the Earth's Spheroidal Surface

Boyd F. Edwards
Department of Physics
Utah State University, Logan, Utah

John M. Edwards
Department of Computer Science
Utah State University, Logan, Utah

(Dated: May 28, 2021)

We explore the forces that shape our spheroidal earth and the forces that govern the motion of a puck that slides without friction on its surface. The earth's stable spheroidal shape (apart from small-scale surface features) is determined by balancing the gravitational forces that hold it together against the centrifugal forces that try to tear it apart. The motion of a puck on its surface differs profoundly from motion on a sphere because the earth's spheroidal deformations neutralize the centrifugal and gravitational forces on the puck, leaving only the Coriolis force to govern the motion. Yet the earth's spheroidal deformations are small and difficult to see in scale drawings. To assist students in exploring the crucial role of these deformations for motion on the earth's surface, we develop a model of uniformly rotating homogeneous earth-like planets with arbitrary eccentricities and arbitrary angular speeds of rotation, derive equations of motion for a puck sliding on the frictionless surface of such a planet, and introduce *CorioVis* software for visualizing this motion. By construction, this model replicates the rotational properties of the reference spheroid that is used in terrestrial cartography, geodesy, and the global positioning system.

I. INTRODUCTION

The motion of a hockey puck on the earth's spheroidal surface differs profoundly from motion on a sphere [1]. Motion on a frictionless sphere is simple; the puck executes uniform circular motion in a great circle around the earth's center, as seen by an inertial observer, and spends equal time in the northern and southern hemispheres [2]. On a frictionless spheroid, the puck executes "inertial oscillations" that generally keep it close to its initial latitude [3–7].

Why? Because the apparent gravitational force, defined as the vector sum of the gravitational and centrifugal forces, is perpendicular to the earth's spheroidal surface at every point on this surface (ignoring small-scale surface features), as seen by an observer in the rotating frame [8]. The earth's spheroidal deformations therefore neutralize the gravitational and centrifugal forces and leave only the velocity-dependent Coriolis force to govern the puck's motion [9, Ch. 6]. Consequently, the puck's kinetic energy is conserved not in the inertial frame, as it is for a spherical earth, but in the rotating frame [1]. These facts are well known in the meteorology and oceanography communities [10–13], but seem to be less appreciated in the physics community.

The earth's spheroidal deformations are small and difficult to see in photographs or scale drawings. In the geodesy literature, the relative difference between the equatorial radius a and the polar radius b of the earth is called the flattening,

$$f = \frac{a-b}{a}. \tag{1}$$

For the values a_r and b_r for the reference spheroid that is used in terrestrial cartography, geodesy, satellite navigation, and the global positioning system, the earth's flattening is $f_\mathrm{r} = 0.0034$ (Table I, [14–17]). This small value belies the crucial role of spheroidal deformations in the motion of objects moving on the earth's surface.

Compounding this problem is a long history of confusion about the Coriolis force, including errors by Richard Feynman and Max Born [8, 18–24]. Hadley's principle is often invoked to explain Coriolis deflections for northward and southward motion, but this principle violates the conservation of axial angular momentum [8, 11, 13, 21, 25–28], as do some studies of objects that are dropped vertically [20, 29, 30]. For both horizontal and vertical motion, conservation of axial angular momentum in the inertial frame is needed to correctly account for Coriolis deflections [31–33].

The centrifugal and Coriolis forces are "inertial" forces

TABLE I. List of constants including symbols, descriptions, equation numbers, and values. The subscript "r" refers to values for the earth's reference spheroid [14–17].

Sym.	Description	Eq.	Value
a_r	equatorial radius	(1)	6378.137 km
b_r	polar radius	(1)	6356.752 km
f_r	flattening	(1)	0.003353
τ_r	period	(2)	23.93 hr
Ω_r	angular speed	(2)	7.292×10^{-5} rad/s
e_r	eccentricity	(14)	0.08182
G	gravitational constant	(19)	$6.674 \times 10^{-11}\,\mathrm{N{\cdot}m^2/kg^2}$
ρ_m	mass density	(20)	7097 kg/m^3

that appear as extra terms in Newton's second law when it is transformed into a rotating reference frame. Instructors of introductory general physics courses generally teach uniform circular motion in the inertial frame, without introducing the rotating frame or the centrifugal force [34]. Students of intermediate (upper-division undergraduate) classical mechanics learn how transform Newton's second law into the rotating frame, and are thereby introduced to the centrifugal and Coriolis forces [35, Ch. 9]. These forces are central to understanding the shape of the earth and motion on its surface [4, 36].

In this paper, we do not address the pedagogy of the centrifugal force [34], and focus instead on its role in shaping the earth and in governing the frictionless motion of a puck on its surface.

Despite evidence that using multiple representations (verbal, mathematical, graphical, pictorial, and analogical) in instruction can increase student performance [37–40], and despite evidence that attending to student interpretations of concepts can increase student interest [41], treatments of the Coriolis force in intermediate mechanics tend to be largely mathematical [35]. Physics students using computer simulations have been shown to outperform their counterparts who use physical equipment or textbooks [42–45]. Yet currently available visualizations of Coriolis phenomena on the rotating earth are restricted to the spherical earth and to one frame of reference [46].

Given the importance of the Coriolis force in meteorology [11, 47], oceanography [12], ballistics [48], and sniping [49] and given the persistent errors, misconceptions, and omissions in the literature, there is a critical need for instructional materials that teach motion on the earth's surface clearly, simply, and correctly, and that engage multiple representations and points of view.

The purpose of this paper is to address this need. We accomplish this by introducing a geodetic model that relates the eccentricity of a homogeneous earth-like planet to its stable angular speed of rotation, together with feature-rich web-based interactive visualization software called *CorioVis* [50]. This software enables students to explore the motion of a puck for their choices of the earth's eccentricity and angular speed of rotation, from both the inertial and rotating frames of reference. We offer this software freely to the physics and earth science communities.

In contrast with other models that assume small spheroidal deformations [51, p. 48][9, Ch. 6], our model and our software describe motion on an earth whose spheroidal eccentricity and angular speeds of rotation are both arbitrary. This generality enables students to see how a puck moves on a planet whose spheroidal deformations are large enough to see, and to explore the consequences of varying the rotation rate and eccentricity.

The earth's reference rotation period of $\tau_\mathrm{r} = 23.93$ h is the time required for the earth to rotate once on its axis with respect to the stars. Because of the earth's orbit around the sun, this period is shorter than the earth's mean solar day of 24 h, the average time required for the earth to rotate once on its axis relative to the sun. The corresponding angular speed of rotation is [14] (Table I)

$$\Omega_\mathrm{r} = \frac{2\pi}{\tau_\mathrm{r}} = 7.292 \times 10^{-5} \text{ rad/s}. \quad (2)$$

Early in its history, the earth was flatter and had a smaller rotation period. This period has increased over time in part because lunar tidal forces have transferred angular momentum from the earth to the moon [36, 52]. Computer models show that shortly after the astronomical impact that is thought to have created the moon, the earth's rotation period might have approached the instability limit of $\tau \approx 2$ h [53].

At least one dwarf planet has significant flattening. Haumea, discovered in 2004, is the third-largest dwarf planet in the solar system after Eris and Pluto [54, 55]. It has flattening $f \approx 0.5$ and rotation period $\tau = 3.9$ h, the smallest period of any known body in the solar system larger than 100 km [56–58].

Our model considers only the roles of the two largest forces in shaping the earth, gravity and the centrifugal force, which are responsible for the 21-km difference between the earth's equatorial and polar radii. We ignore forces associated with geologic activity, which are responsible for smaller-scale surface features such as 8.8-km Mount Everest. We ignore the roles of material properties and tidal forces from nearby celestial bodies [59–61]. The study of the effect of rotation on flattening dates back to Sir Isaac Newton, who proposed $f = 1/230 = 0.0043$ in his *Principia* [62].

Contributions of this paper include: (a) a model of the stable angular speeds of spheroidal earth-like planets of arbitrary eccentricities, (b) a model of the motion of a puck on the surface of such a planet that rotates with arbitrary angular speed, and (c) *CorioVis* simulation and visualization software that is based on these models.

The remainder of this paper is organized as follows: We discuss the geodetic coordinates that are used to describe motion on a spheroid (Sec. II), develop a model of the stable angular speed of a spheroidal earth-like planet of arbitrary eccentricity (Sec. III), review the forces acting on a puck that slides without friction on its surface (Sec. IV), review the conservation laws that apply to this motion (Sec. V), develop the associated equations of motion (Sec. VI), introduce *CorioVis* visualization software (Sec. VII), use *CorioVis* to explore the motion of a puck on a highly eccentric planet (Sec. VIII), and discuss conclusions and future plans (Sec. IX).

II. COORDINATES

We use geodetic coordinates (θ, ϕ) to describe the motion of a puck on the earth's spheroidal surface, with the geodetic latitude θ defined as the angle between the normal direction and the equatorial plane, measured northward from the equator, and with the longitude ϕ measured eastward from the prime meridian. The equato-

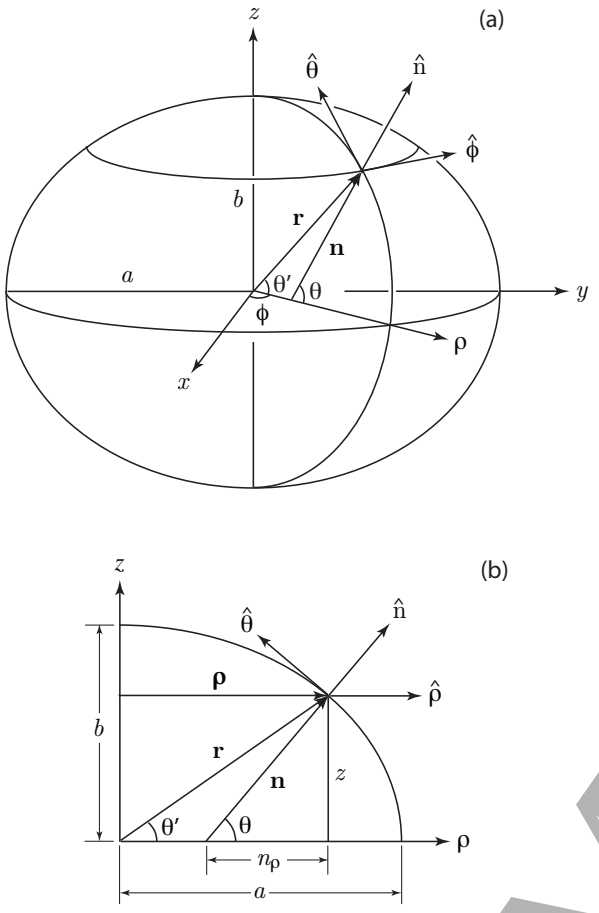

FIG. 1. Geodetic coordinates used to specify points on the surface of the earth, treated as a spheroid with equatorial radius a and polar radius b, in the rotating reference frame (a). As viewed by an earthbound observer in this frame, the unit vectors $\hat{\mathrm{x}}$, $\hat{\mathrm{y}}$, and $\hat{\mathrm{z}}$ are stationary, with $\hat{\mathrm{x}}$ and $\hat{\mathrm{y}}$ marking specific geographical points on the equator and $\hat{\mathrm{z}}$ marking the north pole. Shown for a point on the surface are its position vector $\mathbf{r}$, its normal vector $\mathbf{n}$, its geodetic latitude θ, its geocentric latitude θ', and its longitude ϕ, with orthogonal unit vectors $\hat{\phi}$, $\hat{\theta}$, and $\hat{\mathrm{n}}$ respectively pointing east, north, and up. The vector $\boldsymbol{\rho}$ specifies the equatorial projection of $\mathbf{r}$, with $\hat{\rho}$ pointing away from the axis of rotation. Frame (b) shows the (ρ, z) plane of the spheroid, with $\hat{\phi}$ directed into the page and n_p giving the component of $\mathbf{n}$ along the ρ axis.

rial radius a is assumed to be independent of longitude. The geodetic latitude θ is more convenient mathematically than the geocentric latitude θ', defined as the angle between the line to the earth's center and the equatorial plane (Fig. 1). When used without qualification, the term "latitude" refers to the geodetic latitude θ, which is used for GPS coordinates and cartography [63].

In this section, we derive the transformation between geodetic and Cartesian coordinates [17, 64] and identify unit vectors that facilitate our treatment of motion on the earth's surface.

In Cartesian coordinates, the position of a puck on the surface of a rotating spheroidal earth is given by

$$\mathbf{r} = x\hat{\mathrm{x}} + y\hat{\mathrm{y}} + z\hat{\mathrm{z}}, \tag{3}$$

where the unit vectors $\hat{\mathrm{x}}$, $\hat{\mathrm{y}}$, and $\hat{\mathrm{z}}$ rotate with the earth, as seen by an observer in the inertial frame. As seen by an observer in the rotating frame, these vectors are stationary and point toward specific, unchanging geographical locations on the earth's surface, with $\hat{\mathrm{x}}$ marking the intersection of the prime meridian and the equator, located off the west coast of Africa, $\hat{\mathrm{y}}$ marking the $\phi = 90°$ east latitude position on the equator, located in the Indian Ocean, and $\hat{\mathrm{z}}$ marking the north pole and defining the earth's rotation axis.

A spheroid is defined as an ellipsoid with two semi-axes of equal length, which we take in the x and y directions. With the unequal semi-axis in the z direction, we write

$$\frac{x^2 + y^2}{a^2} + \frac{z^2}{b^2} = 1, \tag{4}$$

where a is the semi-major axis, or equatorial radius, and b is the semi-minor axis, or polar radius. For an oblate spheroid, $a > b$ [65].

The purpose of this section is to express x, y, and z as functions of θ and ϕ for points on the earth's spheroidal surface. To this end, it is convenient to combine the equatorial components of $\mathbf{r}$ into a vector

$$\boldsymbol{\rho} = x\hat{\mathrm{x}} + y\hat{\mathrm{y}} \tag{5a}$$
$$= \rho\cos\phi\,\hat{\mathrm{x}} + \rho\sin\phi\,\hat{\mathrm{y}} \tag{5b}$$

that points away from the axis of rotation, whose magnitude $\rho = |\boldsymbol{\rho}|$ is the distance from this axis to the point of interest on the earth's surface. It is also helpful to define a normal vector

$$\mathbf{n} = n_\rho\hat{\rho} + z\hat{\mathrm{z}} \tag{6a}$$
$$= n\cos\theta\,\hat{\rho} + n\sin\theta\,\hat{\mathrm{z}} \tag{6b}$$

of magnitude n that points from the equatorial plane to the point of interest on the surface, measured along the direction normal to this surface (Fig. 1b). Accordingly, Eq. (4) becomes

$$\frac{\rho^2}{a^2} + \frac{z^2}{b^2} = 1, \tag{7}$$

implying that every cross section of the spheroid that includes the z axis is an ellipse with semi-major axis a and semi-minor axis b. The spheroid is therefore an "ellipsoid of revolution" [65].

We differentiate Eq. (7) to find the slope of the tangent to the ellipse,

$$\frac{dz}{d\rho} = -\frac{b^2}{a^2}\frac{\rho}{z}, \tag{8a}$$

and the slope of the normal to the ellipse,

$$-\frac{d\rho}{dz} = \frac{a^2}{b^2}\frac{z}{\rho}. \tag{8b}$$

According to Fig. 1b, we can set this slope equal to z/n_ρ, and the ρ component of $\mathbf{n}$ becomes

$$n_\rho = \frac{b^2}{a^2}\rho, \tag{9}$$

whence Eqs. (6) give

$$\rho = \frac{a^2}{b^2} n\cos\theta \tag{10a}$$

$$z = n\sin\theta. \tag{10b}$$

Substituting Eqs. (10) into Eq. (7) yields

$$n = \frac{\left(1-e^2\right)a}{\sqrt{1-e^2\sin^2\theta}}, \tag{11}$$

where

$$e = \frac{\sqrt{a^2-b^2}}{a} \tag{12}$$

is the spheroidal eccentricity. Equation (1) gives a relationship between the eccentricity and the flattening,

$$e^2 = 1-(1-f)^2. \tag{13}$$

Both e and f range between zero and one. For the reference spheroid, the eccentricity is (Table I) [14–16]

$$e_{\rm r} = \frac{\sqrt{a_{\rm r}^2-b_{\rm r}^2}}{a_{\rm r}} = 0.08182. \tag{14}$$

Finally, substituting Eq. (11) into Eqs. (10) gives ρ and z as functions of θ,

$$\rho = \frac{a\cos\theta}{\sqrt{1-e^2\sin^2\theta}} \tag{15a}$$

$$z = \frac{a\left(1-e^2\right)\sin\theta}{\sqrt{1-e^2\sin^2\theta}}. \tag{15b}$$

Figure 1b demands that $z = \rho\tan\theta' = n_\rho\tan\theta$, whence Eqs. (9) and (12) give

$$\tan\theta' = \left(1-e^2\right)\tan\theta. \tag{16}$$

Using Eqs. (5b) and (6b), we define unit vectors by

$$\hat\rho = \frac{\boldsymbol{\rho}}{\rho} = \cos\phi\,\hat{\rm x} + \sin\phi\,\hat{\rm y} \tag{17a}$$

$$\hat{\rm n} = \frac{\mathbf{n}}{n} = \cos\theta\,\hat\rho + \sin\theta\,\hat{\rm z} \tag{17b}$$

$$\hat\theta = \frac{d\hat{\rm n}}{d\theta} = -\sin\theta\,\hat\rho + \cos\theta\,\hat{\rm z} \tag{17c}$$

$$\hat\phi = \frac{d\hat\rho}{d\phi} = -\sin\phi\,\hat{\rm x} + \cos\phi\,\hat{\rm y}, \tag{17d}$$

with derivatives carried out with $\hat{\rm x}$, $\hat{\rm y}$, and $\hat{\rm z}$ held fixed. Equations (17b) and (17c) yield

$$\hat\rho = -\sin\theta\,\hat\theta + \cos\theta\,\hat{\rm n}. \tag{17e}$$

The unit vectors $\hat\phi$, $\hat\theta$, and $\hat{\rm n}$ form an orthogonal right-handed geodetic coordinate system, and respectively point east, north, and up (Fig. 1). Thus, Eq. (3) becomes

$$\mathbf{r} = \rho\hat\rho + z\hat{\rm z} \tag{18a}$$

$$= \rho\cos\phi\,\hat{\rm x} + \rho\sin\phi\,\hat{\rm y} + z\hat{\rm z}, \tag{18b}$$

with ρ and z given by Eqs. (15). Equation (18b) gives the Cartesian coordinates (x, y, z) of a point with latitude θ and longitude ϕ on the earth's spheroidal surface, and reduces to spherical coordinates for $e = 0$.

III. STABLE ANGULAR SPEED

In this section, we use a relationship between the shape of a uniformly rotating homogeneous fluid body and its stable angular speed to develop a model of earth-like planets of arbitrary eccentricity. This model replicates the rotational properties of the earth's reference spheroid and extends to flatter, faster-rotating planets.

We consider a uniformly rotating self-gravitating homogeneous fluid body that finds its stable spheroidal shape by balancing the gravitational forces that hold it together against the centrifugal forces that try to tear it apart. This shape is called the MacLaurin spheroid. In 1742, MacLaurin obtained a relationship [66–70]

$$\frac{\tilde\Omega^2(e)}{2\pi G\rho_{\rm m}} = \frac{\sqrt{1-e^2}}{e^3}\left(3-2e^2\right)\sin^{-1}e - \frac{3}{e^2}\left(1-e^2\right) \tag{19}$$

between the spheroid's eccentricity e, its stable angular speed of rotation $\tilde\Omega$, its mass density $\rho_{\rm m}$, assumed uniform, and the universal gravitational constant G [71].

The earth's mass density varies from about 3,000 kg/m^3 in the crust to about 13,000 kg/m^3 in the core, and has an average value of about 5500 kg/m^3 [72]. Inserting $\rho_{\rm m} = 5500$ kg/m^3 and $e = 0.08182$ from Eq. (14) into Eq. (19) yields $\tilde\Omega = 6.4\times10^{-5}$ rad/s, which underestimates the earth's reference angular speed of rotation given by Eq. (2). This difference stems from: (a) the model's neglect of variations in the earth's mass density and material properties, (b) the inverse square dependence of the gravitational force on distance, and (c) the model's neglect of tidal forces from nearby celestial bodies [59–61, 67, 70].

To match the earth's rotational properties while preserving the simplicity of the homogeneous model, we determine ρ_m by inserting the values of Eqs. (2) and (14) into Eq. (19), which gives

$$\rho_{\rm m} = 7097 \text{ kg/m}^3. \tag{20}$$

This value falls within the earth's mass density range.

Figure 2 shows the stable angular speed $\tilde\Omega(e)$ vs. the eccentricity e using the value of $\rho_{\rm m}$ given by Eq. (20). This angular speed reaches a maximum $\tilde\Omega(e_{\rm m})$ at $e_{\rm m} = 0.9300$, above which flattened spheroids rotate more slowly than

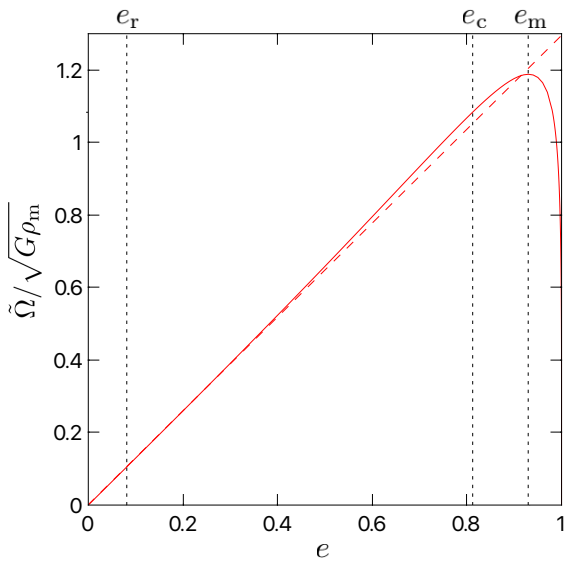

FIG. 2. Plot of the scaled stable angular speed of rotation $\tilde{\Omega}/\sqrt{G\rho_{\rm m}}$ vs. the spheroidal eccentricity e for the homogeneous self-gravitating fluid model of earth-like planets given by Eqs. (19) and (20) (solid trace), together with its $e \to 0$ limit given by Eq. (21) (dashed trace). Also shown are the earth's reference eccentricity $e_{\rm r}$, the critical eccentricity $e_{\rm c}$, and the eccentricity $e_{\rm m}$ at which $\tilde{\Omega}$ reaches its maximum.

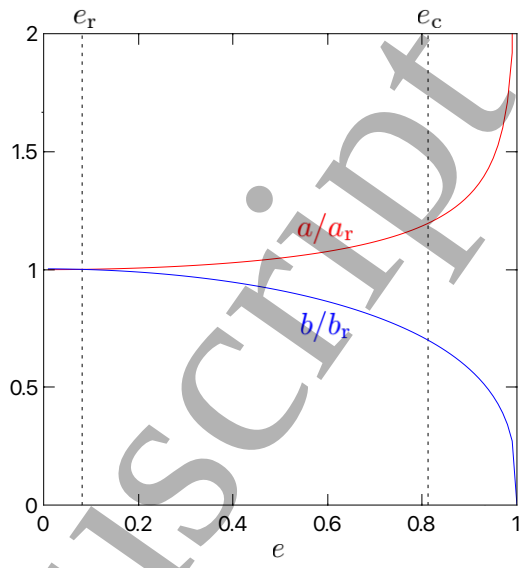

FIG. 3. Plot of the ratio $a/a_{\rm r}$ of the equatorial radius a to the reference equatorial radius $a_{\rm r}$ and the ratio $b/b_{\rm r}$ of the polar radius b to the reference polar radius $b_{\rm r}$ vs. the eccentricity e, from Eqs. (23). Indicated also are the reference and critical eccentricities, $e_{\rm r}$ and $e_{\rm c}$.

this maximum speed. Above $e_{\rm c} = 0.8127$, MacLaurin spheroids are unstable to perturbations that convert them into Jacobi ellipsoids [68, 70]. MacLaurin spheroids are stable over the range $0 \le e \le e_{\rm c}$, which is sufficient for our pedagogical purposes. Also shown in Fig. 2 is the $e \to 0$ limit

$$\tilde{\Omega}(e) = 2\sqrt{\frac{2\pi G\rho_{\rm m}}{15}}\,e, \tag{21}$$

which agrees with Eq. (19) to within 3% over this range.

We also require that the spheroid of eccentricity e have the same volume as the reference spheroid by setting

$$V = \frac{4}{3}\pi a^2 b = \frac{4}{3}\pi a_{\rm r}^2 b_{\rm r}. \tag{22}$$

Combining Eqs. (12), (14) and (22) yields the equatorial and polar radii, a and b, for a spheroid of eccentricity e whose volume is the same as the reference spheroid,

$$a = a_{\rm r}\left(\frac{1-e_{\rm r}^2}{1-e^2}\right)^{1/6} \tag{23a}$$

$$b = b_{\rm r}\left(\frac{1-e^2}{1-e_{\rm r}^2}\right)^{1/3}. \tag{23b}$$

For $e = 0$, Eqs. (14) and (23) give the result $a = b$ for a sphere. Figure 3 is a plot of $a/a_{\rm r}$ and $b/b_{\rm r}$ vs. the eccentricity e, with $a/a_{\rm r} = b/b_{\rm r} = 1$ at $e = e_{\rm r}$, and with $a/a_{\rm r} = 1.20$ and $b/b_{\rm r} = 0.70$ at $e = e_{\rm c}$.

In summary, we model the earth and earth-like planets of arbitrary eccentricities e as MacLaurin spheroids of uniform mass density $\rho_{\rm m} = 7097$ kg/m^3 whose stable angular speeds of rotation $\tilde{\Omega}(e)$ are given by Eq. (19) and whose equatorial and polar radii are given by Eqs. (23). Evaluated at the earth's reference eccentricity $e_{\rm r}$, the model recovers the earth's angular speed $\Omega_{\rm r}$, equatorial radius $a_{\rm r}$, and polar radius $b_{\rm r}$ (Table I).

To facilitate a complete understanding of the role of the earth's shape for motion on its surface, we also consider planets that rotate at angular speeds Ω that differ from their stable angular speed $\tilde{\Omega}(e)$. For this purpose, once the stable spheroidal shape with eccentricity e and angular speed $\tilde{\Omega}(e)$ has been achieved, we freeze the earth into a rigid undeformable body of eccentricity e, and then consider the consequences of changing its angular speed. In this way, we can consider angular speeds Ω that are smaller than, equal to, or larger than $\tilde{\Omega}(e)$.

IV. FORCES

We now consider the forces on a puck that slides on the surface of a rotating spheroidal planet of eccentricity e. The planet rotates with angular speed Ω, which may or may not coincide with the stable angular speed $\tilde{\Omega}(e)$ given by Eq. (19).

As seen by an observer in an inertial frame S_0, that is, as seen by an observer who looks down from space upon the rotating spheroidal earth, a puck of mass m that slides without friction along its surface satisfies Newton's

second law,

$$m\left(\frac{d^2\mathbf{r}}{dt^2}\right)_{S_0} = \mathbf{F}_\mathrm{g} + \mathbf{F}_\mathrm{n}. \tag{24}$$

Here $\mathbf{F}_\mathrm{g} = m\mathbf{g}$ and $\mathbf{F}_\mathrm{n} = -F_\mathrm{n}\hat{\mathrm{n}}$ are the gravitational and normal forces on the puck, $\mathbf{g}$ is its gravitational acceleration, $\mathbf{r}$ is its position, and $(d^2\mathbf{r}/dt^2)_{S_0}$ is its acceleration.

We also consider a non-inertial frame S that rotates with the earth's angular velocity $\mathbf{\Omega} = \Omega\hat{\mathrm{z}}$ relative to the inertial frame. Transforming Eq. (24) into the rotating frame gives [1]

$$m\left(\frac{d^2\mathbf{r}}{dt^2}\right)_{S} = \mathbf{F}_\mathrm{g} + \mathbf{F}_\mathrm{n} + \mathbf{F}_\mathrm{cor} + \mathbf{F}_\mathrm{cen}, \tag{25}$$

where the Coriolis force $\mathbf{F}_\mathrm{cor} = -2m\mathbf{\Omega}\times(d\mathbf{r}/dt)_S$ and the centrifugal force $\mathbf{F}_\mathrm{cen} = -m\mathbf{\Omega}\times(\mathbf{\Omega}\times\mathbf{r})$ are "inertial" forces that apply only in the rotating frame. In this frame, $(d^2\mathbf{r}/dt^2)_S$ is the acceleration and $(d\mathbf{r}/dt)_S = v_\phi\,\hat{\phi} + v_\theta\,\hat{\theta}$ is the velocity, with eastward and northward components

$$v_\phi = \rho\frac{d\phi}{dt} \tag{26a}$$

$$v_\theta = R\frac{d\theta}{dt}, \tag{26b}$$

where

$$R = \frac{\left(1-e^2\right)a}{\left(1-e^2\sin^2\theta\right)^{3/2}} \tag{27}$$

is the earth's meridional radius of curvature, measured along a line of longitude. In Eq. (25), the Coriolis and centrifugal forces augment the normal and gravitational forces that also apply in the inertial frame.

The apparent gravitational force $\mathbf{F}'_\mathrm{g} = \mathbf{F}_\mathrm{g} + \mathbf{F}_\mathrm{cen}$ is defined as the vector sum of the gravitational and centrifugal forces, and is perpendicular to the surface of a stably rotating planet at every point on its surface [8].

V. CONSERVATION LAWS

As seen by an observer in the inertial frame S_0, the torques on the puck have no components in the axial direction and the axial component of the puck's angular momentum is therefore conserved [1]. This component is given by

$$(L_z)_{S_0} = m\rho\left(\Omega\rho + v_\phi\right), \tag{28}$$

where the puck's eastward velocity $\Omega\rho + v_\phi$ in the inertial frame is the sum of the earth's tangential velocity $\Omega\rho$ and the puck's eastward velocity v_ϕ in the rotating frame.

As seen by an earthbound observer in the rotating frame S, the kinetic energy of the puck is given by

$$(T)_S = \frac{1}{2}m\left(v_\phi^2 + v_\theta^2\right). \tag{29}$$

The time rate of change of this energy is given by [1]

$$\frac{d}{dt}(T)_S = m\left(\tilde{\Omega}^2 - \Omega^2\right)\rho v_\theta\sin\theta, \tag{30}$$

Thus, for stably rotating planets with $\Omega = \tilde{\Omega}(e)$, the puck's kinetic energy is conserved in the rotating frame because the associated forces do no net work on the puck.

VI. EQUATIONS OF MOTION

We now construct equations of motion from these conservation laws. To build dimensionless constants, we consider a puck of mass m that is at rest at the equator as seen by a rotating observer on an earth-like planet of arbitrary eccentricity e that rotates at the earth's reference angular speed Ω_r. As seen by an inertial observer, this puck has tangential speed $a\Omega_\mathrm{r}$, angular momentum $ma^2\Omega_\mathrm{r}$, and kinetic energy $ma^2\Omega_\mathrm{r}^2/2$.

We accordingly define a dimensionless axial angular momentum in the inertial frame,

$$\mathcal{L} = \frac{(L_z)_{S_0}}{ma^2\Omega_\mathrm{r}}, \tag{31a}$$

and a dimensionless kinetic energy in the rotating frame,

$$\mathcal{T} = \frac{2\,(T)_S}{ma^2\Omega_\mathrm{r}^2}. \tag{31b}$$

These definitions, together with Eqs. (15a), (26), and (27), allow us to write Eqs. (28), (29), and (30) as

$$\mathcal{L} = \frac{\cos^2\theta}{1-e^2\sin^2\theta}\left(\frac{\Omega+\dot{\phi}}{\Omega_\mathrm{r}}\right) \tag{32a}$$

$$\mathcal{T} = \frac{\cos^2\theta}{1-e^2\sin^2\theta}\left(\frac{\dot{\phi}^2}{\Omega_\mathrm{r}^2}\right) + \frac{\left(1-e^2\right)^2}{\left(1-e^2\sin^2\theta\right)^3}\left(\frac{\dot{\theta}^2}{\Omega_\mathrm{r}^2}\right) \tag{32b}$$

$$\dot{\mathcal{T}} = \left(\frac{\tilde{\Omega}^2-\Omega^2}{\Omega_\mathrm{r}^2}\right)\frac{\left(1-e^2\right)\sin 2\theta}{\left(1-e^2\sin^2\theta\right)^2}\,\dot{\theta}, \tag{32c}$$

where the overdot denotes d/dt.

It is convenient to rewrite Eqs. (32) as a system of three coupled first-order nonlinear differential equations,

$$\dot{\phi} = \Omega_\mathrm{r} f_1 \tag{33a}$$

$$\dot{\theta} = \Omega_\mathrm{r} f_2 \tag{33b}$$

$$\dot{\mathcal{T}} = \Omega_\mathrm{r} f_3, \tag{33c}$$

where

$$f_1 = \frac{1 - e^2 \sin^2\theta}{\cos^2\theta}\mathcal{L} - \frac{\Omega}{\Omega_\mathrm{r}} \tag{33d}$$

$$f_2 = \pm\frac{\left(1 - e^2\sin^2\theta\right)^{3/2}}{1 - e^2}\sqrt{f_4} \tag{33e}$$

$$f_3 = \left(\frac{\tilde{\Omega}^2 - \Omega^2}{\Omega_\mathrm{r}^2}\right)\frac{\left(1 - e^2\right)\sin 2\theta}{\left(1 - e^2\sin^2\theta\right)^2}\, f_2 \tag{33f}$$

$$f_4 = \mathcal{T} - \frac{\cos^2\theta}{1 - e^2\sin^2\theta} f_1^2 \tag{33g}$$

are dimensionless functions of θ and $\mathcal{T}$, and where f_2 takes the sign of $\dot{\theta}$.

The general three-dimensional system of Eqs. (33) describes the time evolution of the longitude $\phi(t)$, the geodetic latitude $\theta(t)$, and the dimensionless kinetic energy $\mathcal{T}(t)$ in the rotating frame [Eq. (32b)] for a hockey puck that moves without friction on the surface of a homogeneous earth-like body of arbitrary spheroidal eccentricity e and arbitrary angular speed of rotation Ω. The stable angular speed $\tilde{\Omega}$ depends on e, and is given by Eq. (19). The earth's reference angular speed Ω_r is given in Table I. The dimensionless axial angular momentum $\mathcal{L}$ in the inertial frame is a constant of the motion, and is given by Eq. (32a).

We now consider three special cases.

Case 1: Stably rotating earth of arbitrary eccentricity. For an earth-like body of arbitrary eccentricity e whose angular speed Ω matches its stable angular speed $\tilde{\Omega}$, Eqs. (33c) and (33f) demand that $\dot{\mathcal{T}} = 0$. Accordingly, $\mathcal{T}$ is a constant of the motion given by Eq. (32b), and Eqs. (33) reduce to a two-dimensional system of equations in $\phi(t)$ and $\theta(t)$,

$$\dot{\phi} = \Omega_\mathrm{r} f_1 \tag{34a}$$

$$\dot{\theta} = \Omega_\mathrm{r} f_2, \tag{34b}$$

with f_1 and f_2 given by Eqs. (33d) and (33e).

Case 2: Stably rotating weakly spheroidal earth. An approximate two-dimensional system of equations for weakly spheroidal earths can be obtained by setting $e = 0$ in Eqs. (34), yielding

$$\dot{\phi} = \Omega_\mathrm{r} f_1 \tag{35a}$$

$$\dot{\theta} = \Omega_\mathrm{r} f_2, \tag{35b}$$

where

$$f_1 = \mathcal{L}\sec^2\theta - \frac{\Omega}{\Omega_\mathrm{r}} \tag{35c}$$

$$f_2 = \pm\sqrt{\mathcal{T} - \left(\mathcal{L}\sec\theta - \frac{\Omega}{\Omega_\mathrm{r}}\cos\theta\right)^2}, \tag{35d}$$

with constants of the motion given by

$$\mathcal{L} = \left(\frac{\Omega + \dot{\phi}}{\Omega_\mathrm{r}}\right)\cos^2\theta \tag{35e}$$

$$\mathcal{T} = \frac{\dot{\phi}^2}{\Omega_\mathrm{r}^2}\cos^2\theta + \frac{\dot{\theta}^2}{\Omega_\mathrm{r}^2}. \tag{35f}$$

This weakly spheroidal approximation serves as the basis for previous investigations of motion on the earth's surface [5, 73–76]. In this approximation, the earth's eccentricity is considered to be nonzero in order to conserve the kinetic energy $\mathcal{T}$ in the *rotating* frame, and is considered to be zero otherwise. For motion on the earth's surface, the weakly spheroidal approximation agrees with the general case described by Eqs. (33) to within 0.1%.

Case 3: Spherical earth. For a spherical earth with $e = 0$, the stable angular speed $\tilde{\Omega} = 0$ vanishes through Eq. (21). Consequently, such an earth cannot rotate stably at any nonzero angular speed Ω, and $\mathcal{T}$ is not conserved at any nonzero angular speed. Setting $e = 0$ in Eqs. (33) yields

$$\dot{\phi} = \Omega_\mathrm{r} f_1 \tag{36a}$$

$$\dot{\theta} = \Omega_\mathrm{r} f_2 \tag{36b}$$

$$\dot{\mathcal{T}} = -\frac{\Omega^2}{\Omega_\mathrm{r}} f_2 \sin 2\theta, \tag{36c}$$

with f_1, f_2, $\mathcal{L}$, and $\mathcal{T}$ given by Eqs. (35c)-(35f). Equations (36) are identical to Eqs. (35) except for Eq. (36c), which governs the time dependence of $\mathcal{T}$. For the spherical earth, the kinetic energy is conserved in the *inertial* frame [1], in which the puck executes uniform circular motion in great circles around the center of the earth [2]. Such eminently simple motion bears little resemblance to motion on our weakly spheroidal earth.

VII. *CORIOVIS* SIMULATIONS

In this section, we introduce *CorioVis* simulation and visualization software as a feature-rich pedagogical tool for exploring the motion of a puck on the surface of a frictionless spheroidal earth-like planet of arbitrary eccentricity e and of arbitrary angular speed of rotation Ω, in both the inertial and rotating reference frames [50].

A. Inputs

CorioVis software integrates Eqs. (33) using the fourth-order Runga-Kutta algorithm with a time step Δt that is fixed except near latitude extrema and pole crossings. The inputs are:

1. Spheroidal eccentricity, e
2. Angular speed of rotation (rad/s), Ω
3. Initial latitude (deg), θ_0

4. Initial longitude (deg), ϕ_0
5. Initial northward velocity (m/s), $v_{\theta 0}$.
6. Initial eastward velocity (m/s), $v_{\phi 0}$
7. Simulation speed / time step (s), Δt

For Input 1, the user may enter an arbitrary value for the eccentricity e, may click a button to set the eccentricity to its reference value $e_{\rm r} = 0.08182$ (Table I), or may click a button to set $e = 0$ (for a spherical earth). For Input 2, the user may enter an arbitrary value for Ω or may click a button to set this ratio to its stable value $\tilde{\Omega}(e)$ given by Eq. (19). Inputs 3 and 4 are the initial latitude $\theta(0) = \theta_0$ and the initial longitude $\phi(0) = \phi_0$, both measured in degrees. Inputs 5 and 6 are the initial northward velocity $v_{\theta 0}$ and the initial eastward velocity $v_{\phi 0}$, both measured in meters per second. The initial values $\dot{\theta}_0$ and $\dot{\phi}_0$ follow from Eqs. (15a), (23a), (26), and (27), and the initial values $\mathcal{L}_0$ and $\mathcal{T}_0$ follow from Eqs. (32a) and (32b).

If the user specifies that the earth rotates at its stable angular speed $\Omega = \tilde{\Omega}(e)$, then $f_3 = \dot{\mathcal{T}} = 0$ and $\mathcal{T}$ is constant. In this case, both the axial angular momentum in the inertial frame and the kinetic energy in the rotating frame are conserved, and the corresponding values $\mathcal{L} = \mathcal{L}_0$ and $\mathcal{T} = \mathcal{T}_0$ remain constant throughout the simulation. If the user specifies some other angular speed, only $\mathcal{L} = \mathcal{L}_0$ is conserved, and Eq. (33c) tracks the time evolution of $\mathcal{T}$.

If $\dot{\theta}_0 \neq 0$, then its sign determines the initial sign of f_2 in Eq. (33e). The Runge-Kutta method fails for $\dot{\theta}_0 = 0$, for which we set $\dot{\theta}_0 = \pm 1 \times 10^{-10}$, with its sign determined by the sign of the initial northward component of the net force [1, from Eqs. (26c) and (40)]

$$\hat{\theta} \cdot \mathbf{F}_{\rm net0} = -m\rho_0 \sin\theta_0 \left(\Omega^2 - \tilde{\Omega}^2 + 2\Omega\dot{\phi}_0\right). \qquad (37)$$

B. Latitude Extrema

We use a binary search-like procedure to find latitude maxima $\theta_{\rm max}$ and minima $\theta_{\rm min}$ where $\dot{\theta} = f_2 = 0$. When the numerical integration overshoots such an extremum and yields a latitude that is outside the allowed range $\theta_{\rm min} \leq \theta \leq \theta_{\rm max}$, the consequence is that $f_4 < 0$ and $\dot{\theta}$ is imaginary by Eq. (33b). Each Runge-Kutta time step requires $\dot{\theta}$ to be evaluated at four different values of θ. Normally, $f_4 \geq 0$ for each of these, and the time step succeeds. If $f_4 < 0$ for one or more of these angles, then θ is near an extremum and the time step fails. After a failed time step, we bisect the time step ($\Delta t \to \Delta t/2$) and try again, integrating until one of these bisected time steps fails, then bisect the time step again, etc. Bisecting N times improves the resolution of the extremum by a factor of 2^N. We typically use $N = 10$, which improves the resolution by a factor of $2^{10} = 1024$. Once an extremum has been found using this search procedure, we reverse the sign of f_2 and continue the integration using the original time step Δt of Input 7.

Our search procedure differs from the classic binary search algorithm in that, while binary search moves in both the positive and negative directions, our procedure only moves forward in time. As a result, our time step does not necessarily bisect at each iteration, as occurs in binary search, affecting the runtime complexity. Instead of the $O(\log n)$ complexity of binary search, our runtime complexity is $O(k \log n)$, where k is the maximum number of iterations between bisections. In practice, $k \leq 2$, reducing our runtime complexity to that of binary search.

C. Near Pole Crossings

Equations (33a) and (33d) give the time rate of change of the longitude, $\dot{\phi}$, which becomes large when the puck passes near a pole ($\theta \approx \pm\pi/2$). To resolve the puck's trajectory when it is close to a pole, we use smaller time steps defined by

$$\Delta t' = \left|\frac{\dot{\phi}_{\rm e}}{\dot{\phi}}\right| \Delta t, \qquad (38)$$

where

$$\dot{\phi}_{\rm e} = \Omega_{\rm r}\mathcal{L} - \Omega \qquad (39)$$

is the time rate of change of the longitude at the equator, found by setting $\theta = 0$ in Eqs. (33a) and (33d). If $|\dot{\phi}| > |\dot{\phi}_{\rm e}|$ at any point in the simulation, then we use the reduced time step $\Delta t'$ instead of the regular time step Δt specified in Input 7. In this way, changes in ϕ that occur during time steps near pole crossings are comparable to changes that occur elsewhere.

The puck reaches a latitude extremum at the point of closest approach to a pole. During the approach to this point, Eq. (38) is used as needed for the integration. When a Runge-Kutta time step fails during this approach, then the binary search-like procedure discussed above is used to refine the estimate of the extremum, using the original time step Δt of Input 7. Once this estimate has been refined, we reverse the sign of f_2 and use Eq. (38) as needed to integrate away from the extremum.

D. Features

CorioVis visualizes the motion of the puck in the reference frame of the user's choice. In the inertial frame, it shows a rotating earth and stationary background stars. In the rotating frame, it shows a stationary earth and moving background stars. The viewing perspective may be changed by clicking and dragging on the image of the earth. *CorioVis* also displays the time-dependent numerical values of the time t, the earth rotation angle Ωt, the puck latitude θ, the puck longitude ϕ, the time rate of change of latitude $\dot{\theta}$, the time rate of change of longitude $\dot{\phi}$, the "relative" puck speed $(v_\phi^2 + v_\theta^2)^{1/2}$ in the

rotating frame, the "absolute" puck speed in the inertial frame, the relative dimensionless kinetic energy $\mathcal{T}$, the absolute dimensionless kinetic energy, and the absolute dimensionless axial angular momentum $\mathcal{L}$.

E. Validation

CorioVis was written by J. Edwards in JavaScript. To validate *CorioVis*, B. Edwards wrote an independent Fortran code to integrate Eqs. (33). The two codes predict values of $\phi(t)$, $\theta(t)$, and $\mathcal{T}(t)$ that agree with each other. As a second validation, we calculate the dynamical values of conserved quantities and compare them with their conserved values, reducing Δt until the differences between the dynamical values and the conserved values are less than 0.1%. For motion on the reference spheroid, this occurs at a time step of about $\Delta t = 50$ s.

VIII. TRAJECTORIES

In this section, we explore the role of the angular speed of rotation of an earth-like planet in the motion of a puck on its surface. We explore this role on a planet of eccentricity $e = 0.6$, whose spheroidal deformations are large enough to see visually, and for angular speeds of rotation $\Omega = 0$, $\Omega = \tilde{\Omega}(e)$, and $\Omega = 2\tilde{\Omega}(e)$. Figure 4 and *CorioVis* Demos 5, 6, and 7 visualize the the puck's motion in these three cases for a puck launched from latitude $\theta_0 = 30°$ and longitude $\phi_0 = 0°$ northward at 250 m/s in the rotating frame, a typical cruising airspeed for commercial passenger aircraft [50, 77].

CorioVis Demo 5 and Fig. 4a illustrate one period of the motion of the puck on an eccentric non-rotating planet ($\Omega = 0$). Such a non-rotating spheroid is not in hydrostatic equilibrium and cannot be liquid, because if it were liquid, then it would form itself into a sphere. Instead, the spheroid must be rigid and undeformable in order to maintain its non-equilibrium shape. Since the planet is not rotating, the inertial and rotating frames are identical, there are no Coriolis and centrifugal forces, and the gravitational force $\mathbf{F}_g$ is identical to the apparent gravitational force $\mathbf{F}'_g$. Were the planet spherical, $\mathbf{F}_g$ would have been perpendicular to the surface at every point on the surface. But for $e = 0.6$, $\mathbf{F}_g$ has a horizontal component that is not balanced by a centrifugal force. This horizontal component causes the puck to oscillate about the north pole with period 4.3 h, reaching its maximum speed of 3400 m/s when it crosses the pole and its minimum speed of 0 m/s at latitude 29.6°.

CorioVis Demo 6 and Fig. 4b illustrate one period of the motion of the puck on an eccentric planet that rotates at its stable angular speed $\Omega = \tilde{\Omega}(e)$. For $e = 0.6$, Eq. (19) gives $\tilde{\Omega}(e) = 7.5\,\Omega_r$, which corresponds to a stable period of rotation of $\tilde{\tau} = 2\pi/\tilde{\Omega}(e) = 3.2$ h. For this planet, $\mathbf{F}'_g$ is perpendicular to the planet at every point on its surface, and the earth's spheroidal deformations

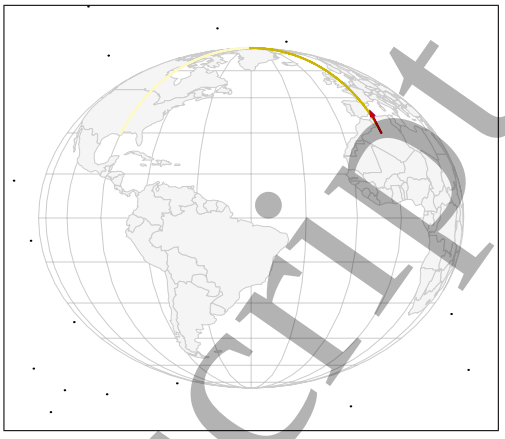

(a) Non-rotating spheroid

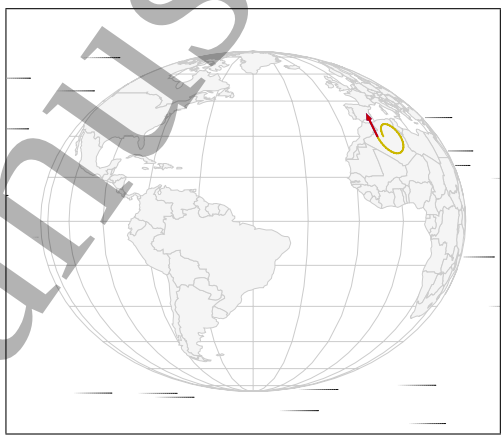

(b) Stably rotating spheroid

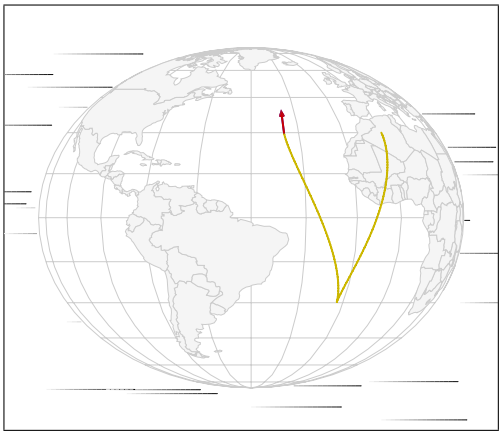

(c) Fast rotating spheroid

FIG. 4. *CorioVis* snapshots of one cycle of the periodic motion of a puck projected northward at 250 m/s, as seen by an observer in the rotating frame on a spheroid of eccentricity $e = 0.6$ and angular speed of rotation $\Omega = 0$ (a), $\Omega = \tilde{\Omega}(e)$ (b), and $\Omega = 2\tilde{\Omega}(e)$ (c), where $\tilde{\Omega}(e)$ is the stable angular speed given by Eq. (19).

neutralize the gravitational and centrifugal forces. Consequently, the motion is governed by the Coriolis force, which acts toward the right in the northern hemisphere. The puck's motion consists of clockwise inertial circles confined between latitudes 24° and 35°, executed at a constant speed of 250 m/s in the rotating frame, with a 3.3-h period of motion and with a small westward drift [1]. The speed is constant because kinetic energy is conserved in the rotating frame (Sec. V). During its first period of motion, the puck tours Algeria and ends 240 km to the west of its starting point.

CorioVis Demo 7 and Fig. 4c illustrate one period of the motion of the puck on an eccentric planet that rotates at an angular speed $\Omega = 2\tilde{\Omega}(e)$ that is twice its stable angular speed, which corresponds to a rotation period of $\tau = 2\pi/\Omega = 1.6$ h. This planet is not in hydrostatic equilibrium, and $\mathbf{F}'_{\rm g}$ drives the puck toward the equator, about which the puck oscillates with a period of 1.7 h. As seen by the rotating observer, the puck reaches its maximum speed of 2700 m/s when it crosses the equator and its minimum speed when it reaches its latitude extremes of $\theta = \pm 30.1°$, where it travels eastward at 12 m/s. The Coriolis force is responsible for the westward drift, which displaces the puck 3800 km to the west during each period of the motion.

IX. CONCLUSIONS

Motion on the earth's surface is important enough to merit treatments and instructional materials that are clear and correct. Because the earth is so nearly spherical, some studies of motion on its surface assume that it is spherical. Yet motion on a spherical earth could not be more different than motion on our spheroidal earth. Accordingly, we develop a spheroidal model that enables us to explore earth-like planets of arbitrary eccentricities and angular speeds of rotation, and deploy this model in studying motion on the surface of the earth. We introduce *CorioVis* software to teach motion on the earth's surface, and make it freely available. These efforts are designed to supplement standard mathematical treatments and to assist students with varying degrees of physics and mathematical preparation in understanding motion on the surface of our earth. We invite educators to use these resources freely in their teaching.

X. ACKNOWLEDGMENTS

We gratefully acknowledge support from U.S. NSF grant No. 1808225, useful discussions with Ryle Briggs, Ridge Cole, Anders Persson, and Hillary Swanson, and *CorioVis* coding by Uttam Khanal.

[1] Boyd F Edwards and John M Edwards. Forces and conservation laws for motion on our spheroidal earth. *in review*, 2021.
[2] David H McIntyre. Using great circles to understand motion on a rotating sphere. *American Journal of Physics*, 68(12):1097–1105, 2000.
[3] Dale R Durran. Is the Coriolis force really responsible for the inertial oscillation? *Bulletin of the American Meteorological Society*, 74(11):2179–2184, 1993.
[4] Anders Persson. Is the Coriolis effect an 'optical illusion'? *Quarterly Journal of the Royal Meteorological Society*, 141(690):1957–1967, 2015.
[5] P Ripa. "Inertial" oscillations and the β-plane approximation(s). *Journal of Physical Oceanography*, 27(5):633–647, 1997.
[6] James R Holton and Gregory J Hakim. *An Introduction to Dynamic Meteorology*, volume 88. Academic Press, 2013.
[7] A Persson. The Coriolis effect: Four centuries of conflict between common sense and mathematics, Part I: A history to 1885. *History of Meteorology*, 2:1–24, 2005.
[8] Anders Persson. How do we understand the Coriolis force? *Bulletin of the American Meteorological Society*, 79(7):1373–1386, 1998.
[9] R Stacey and P Davis. *Physics of the Earth*. Cambridge University Press, 2008.
[10] Jeffrey J Early. The forces of inertial oscillations. *Quarterly Journal of the Royal Meteorological Society*, 138(668):1914–1922, 2012.
[11] Joseph M Moran. *Weather studies: Introduction to atmospheric science*. American Meteorological Society, Boston, Massachusetts, 5th edition, 2012.
[12] David Thomas and David George Bowers. *Introducing Oceanography*. Dunedin Academic Press Ltd, 2012.
[13] Louis J Battan. *Fundamentals of meteorology*. Englewood Cliffs: Prentice-Hall, 2nd edition, 1984.
[14] Helmut Moritz. Geodetic reference system 1980. *Journal of Geodesy*, 74(1):128–133, 2000.
[15] International Association of Geodesy and International Union of Geodesy. *Geodetic reference system 1967*. Number 3. Bureau Central de l'Association Internationale de Géod esie, 1971.
[16] Wikipedia. World Geodetic System. `https://en.wikipedia.org/wiki/World_Geodetic_System#WGS84` (accessed 03-18-2021), 2021.
[17] Bernhard Hofmann-Wellenhof, Herbert Lichtenegger, and James Collins. *Global positioning system: theory and practice*. Springer-Verlag, 1994.
[18] Peder A Tyvand and Kjetil B Haugen. An impulsive bathtub vortex. *Physics of Fluids*, 17(6):062105, 2005.
[19] Martin S Tiersten and Harry Soodak. Dropped objects and other motions relative to the noninertial earth. *American Journal of Physics*, 68(2):129–142, 2000.
[20] Asif Shakur. Debunking Coriolis force myths. *The Physics Teacher*, 52(8):464–465, 2014.
[21] Anders O Persson. Hadley's principle: understanding and misunderstanding the trade winds. *History of Meteorology*, 3:17–42, 2006.

[22] Martin S Tiersten and Harry Soodak. Propagation of a Feynman error on real and inertial forces in rotating systems. *American Journal of Physics*, 66(9):810–811, 1998.

[23] Jack Tessman. Coriolis and consolation. *American Journal of Physics*, 55:392–392, 1987.

[24] Johannes A Van den Akker. Coriolis and consolation. *American Journal of Physics*, 55(12):1063–1063, 1987.

[25] G. Hadley. Concerning the cause of the general trade winds. *Phil. Trans. Roy. Soc. London*, 39:58–62, 1735.

[26] Cleveland Abbe. *The Mechanics of the Earth's Atmosphere: A Collection of Translations*, volume 51 (contains a translation of Hadley's 1735 article). Smithsonian institution, 1910.

[27] Jacques Renault and Emile Okal. Investigating the physical nature of the coriolis effects in the fixed frame. *American Journal of Physics*, 45(7):631–633, 1977.

[28] Brian J Skinner, Stephen C Porter, and Jeffrey Park. *Dynamic earth: an introduction to physical geology*. John Wiley & Sons, 5th edition, 2004.

[29] E Reddingius. Comment on"the eastward deflection of a falling object". *American Journal of Physics*, 52:562–563, 1984.

[30] DR Stirling. Reply to "Comment on 'The eastward deflection of a falling object"'. *American Journal of Physics*, 52(6):563–563, 1984.

[31] Robert Bauman. A Coriolis paradox. *The Physics Teacher*, 21(7):461–462, 1983.

[32] JN Boyd and PN Raychowdhury. Coriolis acceleration without vectors. *American Journal of Physics*, 49:498–499, 1981.

[33] Pirooz Mohazzabi. Free fall and angular momentum. *American Journal of Physics*, 67(11):1017–1020, 1999.

[34] MD Savage and JS Williams. Centrifugal force: fact or fiction? *Physics Education*, 24(3):133, 1989.

[35] John R Taylor. *Classical mechanics*. University Science Books, 2005.

[36] Anders Persson. Mathematics versus common sense: The problem of how to communicate dynamic meteorology. *Meteorological Applications*, 17(2):236–242, 2010.

[37] Patrick B Kohl, David Rosengrant, and Noah D Finkelstein. Strongly and weakly directed approaches to teaching multiple representation use in physics. *Physical Review Special Topics-Physics Education Research*, 3(1):010108, 2007.

[38] Noah S Podolefsky and Noah D Finkelstein. Analogical scaffolding and the learning of abstract ideas in physics: Empirical studies. *Physical Review Special Topics-Physics Education Research*, 3(2):020104, 2007.

[39] Noah S Podolefsky and Noah D Finkelstein. Analogical scaffolding and the learning of abstract ideas in physics: An example from electromagnetic waves. *Physical Review Special Topics-Physics Education Research*, 3(1):010109, 2007.

[40] Noah S Podolefsky and Noah D Finkelstein. Use of analogy in learning physics: The role of representations. *Physical Review Special Topics-Physics Education Research*, 2(2):020101, 2006.

[41] Charles Baily and Noah D Finkelstein. Teaching quantum interpretations: Revisiting the goals and practices of introductory quantum physics courses. *Physical Review Special Topics-Physics Education Research*, 11(2):020124, 2015.

[42] Noah D Finkelstein, Wendy K Adams, CJ Keller, Patrick B Kohl, Katherine K Perkins, Noah S Podolefsky, Sam Reid, and R LeMaster. When learning about the real world is better done virtually: A study of substituting computer simulations for laboratory equipment. *Physical Review Special Topics-Physics Education Research*, 1(1):010103, 2005.

[43] Noah Finkelstein, Wendy Adams, Christopher Keller, Katherine Perkins, Carl Wieman, et al. Hightech tools for teaching physics: The physics education technology project. *Journal of Online Learning and Teaching*, 2(3):110–121, 2006.

[44] Katherine Perkins, Wendy Adams, Michael Dubson, Noah Finkelstein, Sam Reid, Carl Wieman, and Ron LeMaster. PhET: Interactive simulations for teaching and learning physics. *The Physics Teacher*, 44(1):18–23, 2006.

[45] Carl E Wieman, Wendy K Adams, Patricia Loeblein, and Katherine K Perkins. Teaching physics using PhET simulations. *The Physics Teacher*, 48(4):225–227, 2010.

[46] David H McIntyre. Coriolis Force and Noninertial Effects Animations. `http://physics.oregonstate.edu/~mcintyre/coriolis` (accessed 03-18-2021), 2021.

[47] National Geographic. Coriolis Effect. `https://www.nationalgeographic.org/encyclopedia/coriolis-effect/` (accessed 03-18-2021), 2021.

[48] Owen E Thompson. Coriolis deflection of a ballistic projectile. *American Journal of Physics*, 40(10):1477–1483, 1972.

[49] Nicholas Brewster, Tendayi Kerr, Nathan Adams, and Jason Smith. P4_5 bending bullets. *Physics Special Topics*, 10(1), 2011.

[50] John M Edwards and Boyd F Edwards. *CorioVis* Coriolis Visualization Software. `https://edwardsjohnmartin.github.io/coriolis/` (accessed 03-18-2021), 2021.

[51] Alexander L Fetter and John Dirk Walecka. *Theoretical mechanics of particles and continua*. McGraw-Hill, first edition, 1980.

[52] WR Peltier. The history of the earth's rotation: Impacts of deep earth physics and surface climate variability. In Gerald Schubert (editor-in chief), editor, *Treatise on Geophysics, 2nd edition*, chapter 9.09, pages 221–279. Oxford: Elsevier, 2015.

[53] Matija Ćuk and Sarah T Stewart. Making the moon from a fast-spinning earth: a giant impact followed by resonant despinning. *Science*, 338(6110):1047–1052, 2012.

[54] Darin Ragozzine and Michael E Brown. Orbits and masses of the satellites of the dwarf planet Haumea (2003 EL61). *The Astronomical Journal*, 137(6):4766, 2009.

[55] Wikipedia. Dwarf Planet. `https://en.wikipedia.org/wiki/Dwarf_planet` (accessed 8-25-2020), 2020.

[56] David L Rabinowitz, Kristina Barkume, Michael E Brown, Henry Roe, Michael Schwartz, Suzanne Tourtellotte, and Chad Trujillo. Photometric observations constraining the size, shape, and albedo of 2003 EL61, a rapidly rotating, Pluto-sized object in the Kuiper belt. *The Astrophysical Journal*, 639(2):1238, 2006.

[57] Lars Christensen. IAU names fifth dwarf planet Haumea. `https://www.iau.org/news/pressreleases/detail/iau0807/` (accessed 03-18-2021), 2008.

[58] José Luis Ortiz, Pablo Santos-Sanz, B Sicardy, G Benedetti-Rossi, D Bérard, N Morales, R Duffard, F Braga-Ribas, U Hopp, C Ries, et al. The size, shape, density and ring of the dwarf planet Haumea from a stel-

lar occultation. *Nature*, 550(7675):219–223, 2017.

[59] Wolfgang Müller. The effect of rotation on the flattening of celestial bodies: a journey through four centuries. *Mathematics and Mechanics of Complex Systems*, 6(1):1–40, 2018.

[60] Wolfgang H Müller and Wolf Weiss. *The state of deformation in earthlike self-gravitating objects*. Springer, 2016.

[61] Carl D Murray and Stanley F Dermott. *Solar system dynamics*. Cambridge university press, 1999.

[62] A Motte. *Translation of Newton's Principia (1687), Axioms or Laws of Motion, Published by Daniel Adee;* `https://archive.org/details/newtonspmathema00newtrich`*; Principia Book III Proposition XIX Problem III, p. 407 in Motte translation*, 45, 1846.

[63] Wikipedia. Latitude. `https://en.wikipedia.org/wiki/Latitude` (accessed 03-18-2021), 2021.

[64] Wikipedia. Geographic Coordinate Conversion. `https://en.wikipedia.org/wiki/Geographic_coordinate_conversion` (accessed 03-18-2021), 2021.

[65] Wikipedia. Spheroid. `https://en.wikipedia.org/wiki/Spheroid` (accessed 3-18-2021), 2021.

[66] Colin MacLaurin. *A treatise of fluxions: in two books*, volume 1. Ruddimans, 1742.

[67] Subrahmanyan Chandrasekhar. *Ellipsoidal figures of equilibrium*. Yale Univ. Press, 1969.

[68] Raymond Lyttleton. *The stability of rotating liquid masses*. Cambridge University Press, 1953.

[69] Wikipedia. Maclaurin Spheroid. `https://en.wikipedia.org/wiki/Maclaurin_spheroid` (accessed 03-18-2021), 2021.

[70] Eric Poisson and Clifford M Will. *Gravity: Newtonian, post-newtonian, relativistic*. Cambridge University Press, 2014.

[71] Brian Luzum, Nicole Capitaine, Agnès Fienga, William Folkner, Toshio Fukushima, James Hilton, Catherine Hohenkerk, George Krasinsky, Gérard Petit, Elena Pitjeva, et al. The IAU 2009 system of astronomical constants: the report of the IAU working group on numerical standards for Fundamental Astronomy. *Celestial Mechanics and Dynamical Astronomy*, 110(4):293, 2011.

[72] Don L Anderson. *Theory of the Earth*. Blackwell scientific publications, 1989.

[73] P Ripa. Effects of the earth's curvature on the dynamics of isolated objects. part i: The disk. *Journal of physical oceanography*, 30(8):2072–2087, 2000.

[74] P Ripa. Effects of the earth's curvature on the dynamics of isolated objects. part ii: The uniformly translating vortex. *Journal of physical oceanography*, 30(10):2504–2514, 2000.

[75] Nathan Paldor and Peter D Killworth. Inertial trajectories on a rotating earth. *Journal of the atmospheric sciences*, 45(24):4013–4019, 1988.

[76] Nathan Paldor and Andrey Sigalov. The mechanics of inertial motion on the earth and on a rotating sphere. *Physica D: Nonlinear Phenomena*, 160(1-2):29–53, 2001.

[77] Wikipedia. Cruise (aeronautics). `https://en.wikipedia.org/wiki/Cruise_(aeronautics)` (accessed 03-18-2021), 2021.